ACOUSTICS 2012

A comparison between measured and predicted complex intensity in a flanged cylindrical pipe

W. Duan[a], J. Prisutova[b], K. V. Horoshenkov[b] and R. Kirby[a]

[a]Brunel University, Kingston Lane, Uxbridge, UB8 1PH Middlesex, UK
[b]University of Bradford, Great Horton Road, BD7 1DP Bradford, UK
wenbo.duan@brunel.ac.uk

A hybrid finite element method is used to model wave propagation in a flanged cylindrical pipe containing a monopole source. Here, a modal expansion is used to represent sound propagation in the exterior domain and this avoids the use of perfectly matched layers normally found in commercial software packages. Complex intensity in the pipe is then obtained and the real part of the complex intensity is shown to represent the local travelling energy and the imaginary part the local oscillating energy. Results are presented in the plane wave region and at higher frequencies, where the first circumferential mode has cut-on. The predicted complex intensity is then compared to experimental measurements and generally good agreement is observed. From this it is seen that the interaction between the acoustic pressure in the plane wave and the acoustic particle velocity in the first circumferential mode mainly contributes to the transverse flow of energy flow in the pipe, whilst the interaction between the acoustic pressure in the first circumferential mode pressure and the acoustic particle velocity in the first circumferential mode contributes to energy oscillation.

1 Introduction

It is common to see sound intensity used in the measurement of external sound propagation; however, its use for internal problems such as sound propagation in acoustic waveguides is less well developed. Furthermore, sound intensity has traditionally been treated as a real and time independent quantity. Such an approach is feasible in the acoustic far field, where the acoustic particle velocity is in phase with the pressure. In general, however, this is not the case and in the near field of a sound source, or in an acoustic waveguide, one should account for the phase difference between the acoustic particle velocity and the pressure; this can be achieved by treating intensity as a complex quantity.

This article examines complex intensity in a flanged cylindrical pipe, and analyses the influence of the reflection from the flange on the sound intensity field within the duct. Here complex intensity is computed for a monochromatic sound field, where the real part of the complex intensity refers to the magnitude of the local mean energy flow, and the imaginary part to the local oscillatory transport of energy [1]. For a general sound field Jacobsen [2] notes that a number of alternative formulae are available for the complex intensity and he suggests that the method of Heyser [3] may be the most useful. However, a later series of article [4-6] proposes an alternative definition and here Stanzial and Prodi [6] introduce new parameters called the radiating and oscillating intensities in order to distinguish them from the more usual active (real) and reactive (imaginary) terminology [1-3]. This article will review both definitions, with a view to investigating how useful these different definitions are in quantifying sound intensity within a duct. This is to be carried out by comparing theoretical predictions with experimental measurements. The theoretical predictions are generated using a hybrid numerical method of the type described by Kirby [7]. Experimental data is obtained using a "p-u" Microflown transducer [8], which combines a pressure microphone with three particle velocity transducers that simultaneously measure particle velocity in three orthogonal directions.

2 Theory

The complex intensity in a duct is modelled here using a hybrid finite element method based on the method of Kirby [7]. The model includes a sound source located at one end of a circular duct and at the opposite end is an infinite flange, see Figure 1.

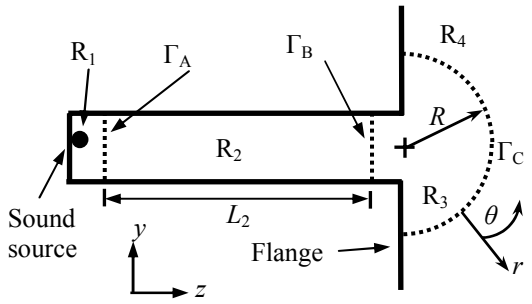

Figure 1: Geometry of flanged duct.

In Figure 1, region R_1 contains the (monopole) sound source, and region R_4 is assumed to extend to infinity (i.e. no reflections are permitted in this region). Region R_3 consists of a section in the pipe joined to a circle of radius R that lies outside of the pipe. The analysis here is restricted to symmetrical problems only and so it is assumed that a two dimensional (Cartesian coordinates) treatment of the problem is sufficient in the duct and *r, θ* for a spherical coordinate system external to the flange. The hybrid mathematical model uses a full finite element discretisation of regions R_1 and R_3, and then uses wave based modal expansions for regions R_2 and R_4. The acoustic wave equation for each region is given as

$$\frac{1}{c_q^2}\frac{\partial^2 p_q}{\partial t^2} - \nabla^2 p_q = 0. \tag{1}$$

Here, p_q is the acoustic pressure, and *c* is the speed of sound in region q, respectively; *t* is time. A monopole source is assumed to be present in R_1, so that the amplitude of this source F_1 is given as,

$$F_1 = \delta(y - y_0)\,\delta(z - z_0)e^{i\omega t}, \tag{2}$$

with y_0, z_0 denoting the location of the monopole source, $i = \sqrt{-1}$, ω the radian frequency and *t* time.

The solution proceeds by first calculating the eigenmodes for R_2 and R_4 and then using mode matching to match continuity of pressure and acoustic particle velocity over planes Γ_A, Γ_B and Γ_C. Accordingly, the sound pressure R_2 is expanded as an infinite sum over the duct eigenmodes, to give

$$p_2(y,z) = \sum_{m=0}^{\infty} A_m \Phi_m(y) \mathrm{e}^{-\mathrm{i}k_0\lambda_m \mathrm{z}} + \sum_{m=0}^{\infty} B_m \Phi_m(y) \mathrm{e}^{+\mathrm{i}k_0\lambda_m \mathrm{z}} \tag{3}$$

$$p_4(r,\theta) = \sum_{n=0}^{\infty} C_n \Psi_n(\theta) \frac{1}{r} \mathrm{e}^{-\mathrm{i}k_0\gamma_n r} \tag{4}$$

Here, A_j, B_m, and C_m, are modal amplitudes, λ_m, is the wavenumber in region R_2 and γ_j, is the wavenumber in region R_4. The quantities $\Phi(x,y)$ and $\Psi(x,y)$ are the eigenfunctions in R_2 and R_4, respectively, and $k_0 = \omega/c_0$.

The hybrid method proceeds by enforcing continuity of acoustic pressure and particle velocity over planes Γ_A, Γ_B and Γ_C. The detailed procedure is described by Kirby [7] and only the final system equations are reported here. The final equation to be solved for the unknown pressures in the system and the modal amplitudes is written as

$$\begin{bmatrix} \mathbf{R_{12}} & \mathbf{R_{13}} \\ \mathbf{R_{31}} & \mathbf{R_{34}} \end{bmatrix} \begin{bmatrix} \mathbf{T_{12}} \\ \mathbf{T_{34}} \end{bmatrix} = \begin{bmatrix} \mathbf{F_1} \\ \mathbf{0} \end{bmatrix}. \tag{5}$$

where, each matrix is given by

$$\mathbf{R_{12}T_{12}} = \begin{bmatrix} \mathbf{G_{1AA}} & \mathbf{G_{1Ae}} & \mathbf{Q_1^T} & -\mathbf{Q_1^T D_1} \\ \mathbf{G_{1eA}} & \mathbf{G_{1ee}} & \mathbf{0} & \mathbf{0} \\ \mathbf{Q_1} & \mathbf{0} & -\mathbf{M_1} & -\mathbf{M_1 D_1} \\ \mathbf{0} & \mathbf{0} & -\mathbf{M_3 D_1} & -\mathbf{M_3} \end{bmatrix} \begin{bmatrix} \mathbf{p_{1A}} \\ \mathbf{p_{1e}} \\ A_n \\ \tilde{B}_n \end{bmatrix} \tag{6}$$

$$\mathbf{R_{34}T_{34}} = \begin{bmatrix} \mathbf{G_{3BB}} & \mathbf{G_{3Be}} & \mathbf{G_{3BC}} & \mathbf{0} \\ \mathbf{G_{3eB}} & \mathbf{G_{3ee}} & \mathbf{G_{3eC}} & \mathbf{0} \\ \mathbf{G_{3CB}} & \mathbf{G_{3Ce}} & \mathbf{G_{3CC}} & \mathbf{Q_4^T} \\ \mathbf{0} & \mathbf{0} & \mathbf{Q_4} & -\mathbf{M_4} \end{bmatrix} \begin{bmatrix} \mathbf{p_{3B}} \\ \mathbf{p_{3e}} \\ \mathbf{p_{3C}} \\ C_n \end{bmatrix} \tag{7}$$

$$\mathbf{R_{13}T_{12}} = \begin{bmatrix} \mathbf{0} & \mathbf{0} & \mathbf{0} & \mathbf{0} \\ \mathbf{0} & \mathbf{0} & \mathbf{0} & \mathbf{0} \\ \mathbf{0} & \mathbf{0} & \mathbf{0} & \mathbf{0} \\ \mathbf{Q_3} & \mathbf{0} & \mathbf{0} & \mathbf{0} \end{bmatrix} \begin{bmatrix} \mathbf{p_{1A}} \\ \mathbf{p_{1e}} \\ A_n \\ \tilde{B}_n \end{bmatrix} \tag{8}$$

$$\mathbf{R_{31}T_{34}} = \begin{bmatrix} \mathbf{0} & \mathbf{0} & -\boldsymbol{Q_3^T D_1} & \boldsymbol{Q_3^T} \\ \mathbf{0} & \mathbf{0} & \mathbf{0} & \mathbf{0} \\ \mathbf{0} & \mathbf{0} & \mathbf{0} & \mathbf{0} \\ \mathbf{0} & \mathbf{0} & \mathbf{0} & \mathbf{0} \end{bmatrix} \begin{bmatrix} \mathbf{p_{3B}} \\ \mathbf{p_{3e}} \\ \mathbf{p_{3C}} \\ \tilde{C}_n \end{bmatrix} \tag{9}$$

$$\mathbf{F_1} = [\mathbf{N_1^T}(y_0, z_0) \quad \mathbf{0} \quad \mathbf{0} \quad \mathbf{0}]^{\mathbf{T}} \tag{10}$$

Here, $[\boldsymbol{D_1}]$ and $[\boldsymbol{D_3}]$ are diagonal matrices with each diagonal element given by $e^{-ik_2\lambda_n L_2}$, $(n = 0,1,\cdots,m_2)$, and $e^{-ik_4\gamma_n R}$, $(n = 0,1,\cdots,m_4)$, respectively; and the modal amplitude coefficients are normalised as $\mathbf{D_1 B} = \tilde{\mathbf{B}}$ and $\mathbf{D_3 C} = \tilde{\mathbf{C}}$. The constituent matrices are given as

$$[\mathbf{G_1}] = \int_{R_1} \left[\nabla \mathbf{N_1^T} \nabla \mathbf{N_1} - k_0^2 \mathbf{N_1^T N_1}\right] dR_1 \tag{11}$$

$$[\mathbf{G_3}] = \int_{R_3} \left[\nabla \mathbf{N_3^T} \nabla \mathbf{N_3} - k_0^2 \mathbf{N_3^T N_3}\right] dR_3 \tag{12}$$

$$[\mathbf{Q_1}] = ik\lambda_m \int_{\Gamma_A} \Phi_m \mathbf{N_1} d\Gamma_A, \quad (m = 0,1,\cdots,m_2) \tag{13}$$

$$[\mathbf{Q_3}] = ik\lambda_m \int_{\Gamma_B} \Phi_m \mathbf{N_3} d\Gamma_B, \quad (m = 0,1,\cdots,m_2) \tag{14}$$

$$[\mathbf{Q_4}] = \left[\frac{ik\gamma_m}{R} + \frac{1}{R^2}\right] \int_{\Gamma_C} \Psi_m \mathbf{N_3} d\Gamma_C, \quad (m = 0,1,\cdots,m_4) \tag{15}$$

$$[\mathbf{M_1}] = ik\lambda_m \int_{\Gamma_A} \Phi_m \Phi_n d\Gamma_A, \quad (m = 0,1,\cdots,m_2; n = 0,1,\cdots,m_2) \tag{16}$$

$$[\mathbf{M_3}] = ik\lambda_m \int_{\Gamma_B} \Phi_m \Phi_n d\Gamma_B \quad (m = 0,1,\cdots,m_2; n = 0,1,\cdots,m_2) \tag{17}$$

$$[\mathbf{M_4}] = \left[\frac{ik\gamma_m}{R^2} + \frac{1}{R^3}\right] \int_{\Gamma_C} \Psi_m \Psi_n d\Gamma_C \quad (m = 0,1,\cdots,m_4; n = 0,1,\cdots,m_4) \tag{18}$$

Here, $\mathbf{N_1}$ and $\mathbf{N_3}$ are the global shape functions in regions R_1 and R_3, respectively. Equation (5) is a set of n_t $(= n_1 + 2m_2 + n_3 + m_4)$ linear equations, where n_1 and n_3 are the number of nodes in regions R_1 and R_3, and m_2 and m_4 are the number of modes in regions R_2 and R_4, respectively. Modal amplitudes and the acoustic pressures are then found on the solution of Eq. (5)

The complex intensity may then be found following the solution Eq. (5). In general the instantaneous active and reactive intensity may be defined as

$$\mathbf{I}(t) = 0.5\mathrm{Re}\{p\mathbf{u}^*\}\left[1 + \cos 2(\omega t + \emptyset_p)\right] \tag{19}$$

and

$$\mathbf{J}(t) = 0.5\mathrm{Im}\{p\mathbf{u}^*\} \sin 2\left(\omega t + \emptyset_p\right). \tag{20}$$

Here, $\mathbf{I}(t)$ and $\mathbf{J}(t)$ are the instantaneous active and reactive intensity, respectively, $\mathbf{u}^*$ is the complex conjugate of the velocity vector $\mathbf{u}$, and $\emptyset_p$ is the phase of the pressure. In R_2 the pressure may then be written as

$$p_2(r,z) = |p_2| e^{i(\omega t + \emptyset_2)} \tag{21}$$

where

$$|p_2|^2 = \sum_{n=0}^{\infty} \Phi_n^2(r,\theta)[\psi_n^2(z) + \varphi_n^2(z)]. \tag{22}$$

and

$$\emptyset_2 = \arctan\left[\frac{\sum_{n=0}^{\infty} \Phi_n(r)\psi_n(z)}{\sum_{n=0}^{\infty} \Phi_n(r)\varphi_n(z)}\right] \tag{23}$$

with

$$\psi_n(z) = [\mathrm{Re}(A_n) + \mathrm{Re}(B_n)] \cos(k\lambda_n z) + [\mathrm{Im}(A_n) - \mathrm{Im}(B_n)] \sin(k\lambda_n z) \tag{24}$$

$$\varphi_n(z) = [\mathrm{Re}(B_n) - \mathrm{Re}(A_n)] \sin(k\lambda_n z) + [\mathrm{Im}(A_n) + \mathrm{Im}(B_n)] \cos(k\lambda_n z). \tag{25}$$

Finally, using the momentum equation, the velocity may be written as

$$u_{2\sigma} = \left(\frac{1}{\rho\omega}\right)\left[-|p_2| \frac{d\emptyset_2}{d\sigma} + i \frac{d|p_2|}{d\sigma}\right] e^{i(\omega t + \emptyset)}, \tag{26}$$

with $\sigma = r$ or z. The instantaneous axial, radial and circumferential active and reactive intensities can then be written as

$$I_\sigma(t) = -\left(\frac{1}{\varepsilon_\sigma \rho\omega}\right)\left[|p_2|^2 \frac{d\emptyset_2}{d\sigma}\right] \cos^2(\omega t + \emptyset_2), \tag{27}$$

and

$$J_\sigma(t) = -\left(\frac{1}{4\varepsilon_\sigma \rho\omega}\right)\left[\frac{d|p_2|^2}{d\sigma}\right]\sin^2(\omega t + \emptyset_2) \qquad (28)$$

where $I_\sigma(t)$ and $J_\sigma(t)$ are instantaneous active and reactive intensities in the direction σ, respectively. The time independent complex intensity may then be calculated by dropping the time dependence from equations (19) and (20) and substituting in the values for pressure and velocity.

3 Results and Discussion

The theoretical predictions are compared here with experimental measurements taken in a harmonic (or monochromatic) sound field. The duct studied is 6 m long and has a diameter of 150 mm. The sound source in the experiment is a loudspeaker that is positioned behind the closed end of the duct and is connected to the duct by a narrow tube so that only the open end of the tube penetrates the far end (in region R_1). This is so the loudspeaker takes on a high acoustic impedance at the (nominally) closed end of the duct. A microflown USP probe [8] is used to measure the acoustic pressure and tri-axial components of the particle velocity.

The experimental complex intensity is calculated in two ways. The first technique is that of Heyser [3], which uses Hilbert transforms to give

$$\boldsymbol{I}(t) = \frac{1}{2}p\boldsymbol{u} + \frac{1}{2}\hat{p}\hat{\boldsymbol{u}} \qquad (29)$$

$$\boldsymbol{J}(t) = \frac{1}{2}\hat{p}\boldsymbol{u} - \frac{1}{2}p\hat{\boldsymbol{u}}, \qquad (30)$$

where, p and $\boldsymbol{u}$ is the recorded time history of pressure and velocity, and $\hat{p}$ and $\hat{\boldsymbol{u}}$ are the Hilbert transform of p and $\boldsymbol{u}$. The second technique is that of Schiffrer and Stanzial [4] and the real and imaginary parts of the complex intensity are called here the radiating and oscillating instantaneous intensity, to give

$$\boldsymbol{I}_{rad}(t) = \frac{p^2\langle p\boldsymbol{u}\rangle}{\langle p^2\rangle} \qquad (31)$$

$$\boldsymbol{J}_{osc}(t) = \frac{\langle p^2\rangle p\boldsymbol{u} - p^2\langle p\boldsymbol{u}\rangle}{\langle p^2\rangle}. \qquad (32)$$

where $\langle\cdot\rangle$ indicates a time averaging process and $\mathbf{I}_{\mathrm{rad}}(t)$ and $\mathbf{I}_{\mathrm{osc}}(t)$ are the radiating and oscillating intensity, respectively [6]. These two techniques can be used to calculate the instantaneous complex intensity, but since they are used here in a monochromatic sound field they can also be used to recover the steady state response.

In Figures 2 and 3, the instantaneous active and reactive intensity is shown for a location coincident with the exit plane of the duct (i.e. at the duct aperture) at an excitation frequency of 1 kHz (which lies within the plane wave regime of the duct). It is seen that theory and experiment generally show good agreement between one another. It is noticeable that the amplitude of the active intensity is much larger than that of the reactive intensity, and this shows that most of the energy radiates out of the duct. In addition, from 0 to 2 ms the experimental complex intensity is not very stable, due to the initial response of the system; however, after this initial period the experimental response settles down and good agreement between prediction and experiment is observed.

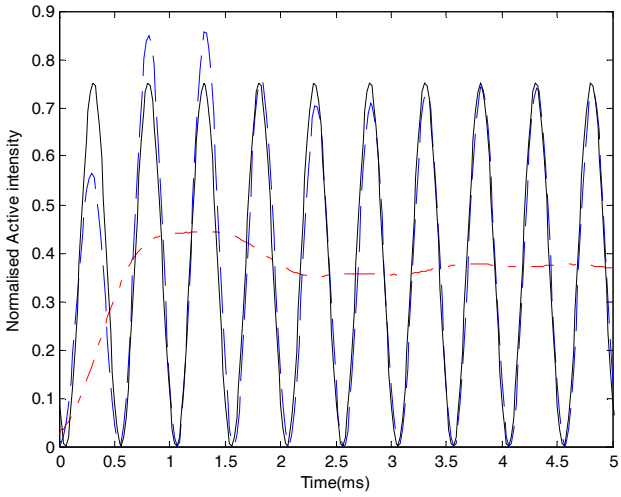

Figure 2: Instantaneous active intensity at 1kHz. ——— theory; - - - - , experiment [4]; - · - · - · - , experiment [3].

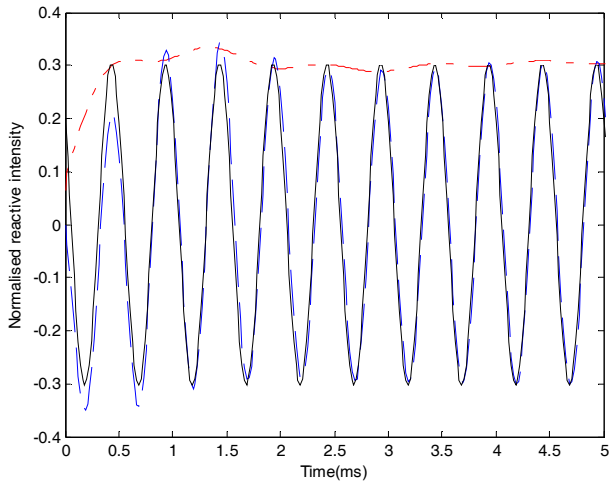

Figure 3: Instantaneous reactive intensity at 1kHz. ——— theory; - - - - , experiment [4]; - · - · - · - , experiment [3].

In Figures 2 and 3 it is evident that the method of Schiffrer and Stanzial [4] agrees well with the theoretical predictions. The method of Heyser [3] cleary delivers a different interpretation of the sound field, and here it appears to act as a running time average for the active intensity, and as an upper envelope for the reactive intensity. Thus, Figures 2 and 3 clearly demonstrate that the method of Schiffrer and Stanzial is of more use when attempting to recover the detailed characteristics of the complex intensity sound field within a duct.

In Figures 4 and 5 the time independent axial active and reactive intensity is plotted as a function of the axial coordinate z (at a frequency of 1 kHz). Here, it is evident that away from the exit plane of the duct the theoretical active intensity is almost constant, whereas closer to the duct exit higher order evanescent modes significantly affect the sound intensity distribution. This near field effect is also seen in the plot of the reactive intensity. It is noticeable also that good agreement between prediction and experiment is generally observed for the time independent

intensity, although some oscillation is evident with the experimental vales for active intensity.

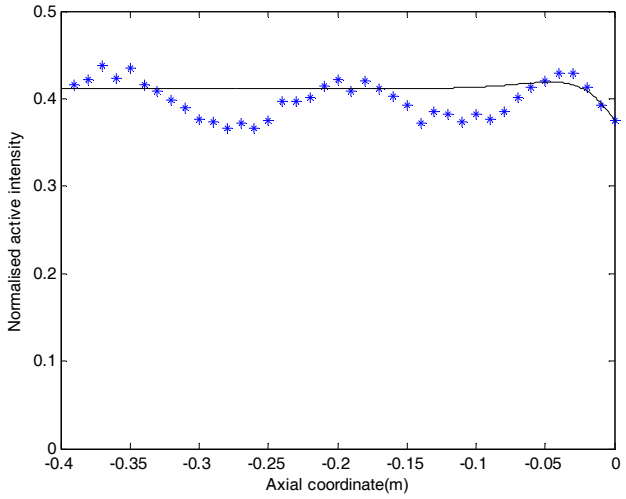

Figure 4: Time independent active intensity
——— theory; * * * * * , measurement.

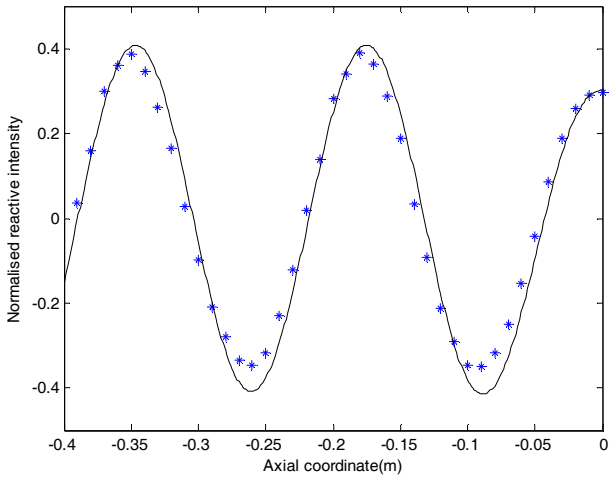

Figure 5: Time independent reactive intensity
——— theory; * * * * * , measurement.

It is interesting to look more closely at the complex intensity patterns close to the flange of the duct and so in Figures 6 and 7 the predicted active and reactive time independent intensity is plotted. Here, the length of the arrow denotes the magnitude of the intensity and in Fig. 6 it can be seen that the magnitude of the active intensity is almost constant inside the duct, and the intensity vectors are all aligned with the z axis. This is caused by the plane wave condtions within the duct and it is only very close to the open end of the duct that the active intensity vectors take on a small radial component. It is noted here that at the sharp corner between the duct and the flange the predicted intensity becomes singular, as the velocity vector transfers from being purely axial to purely radial at the corner in order to maintain the Neumann boundary condition on the wall. It is the presence of evanescent modes at the duct aperture that is responsible for the radial component appearing in the active intensity; however, it is interesting to note that this effect is much more pronounced for the reactive intensity, where the effect of evanescent modes is seen to extend much further into the duct. Thus, it appears that evanescent modes play an important role in the oscillatory behaviour of the sound field close to the open end of the duct. In Figure 7 the magnitude of the reactive intensity outside of the duct is also seen to drop more quickly when compared to the active intensity. This indicates that the oscillating energy decays more quickly than the travelling energy once sound wave exits the duct, which is to be expected as there is no discontinuity or sound source present outside of the duct.

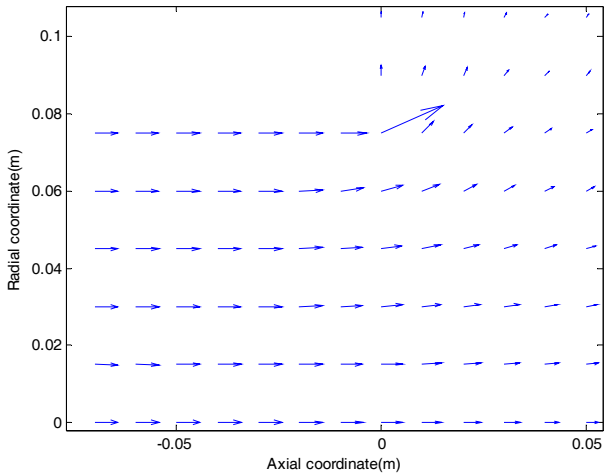

Figure 6: Time-independent active intensity distribution at 1 kHz

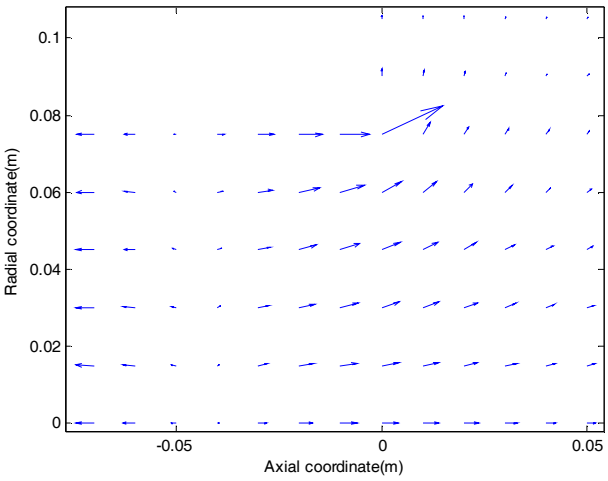

Figure 7: Time-independent reactive intensity distribution at 1 kHz

In Figure 7 the reactive intensity is seen to reduce to approximately zero at a distance of roughly 44 mm from the end of the duct. This has a physical significance, as the reactive intensity vector is normal to the surfaces of constant pressure and points in the direction of decreasing pressure. The reactive intensity thus reveals the anti-node position of the acoustic intensity for the duct. This means that the end correction for the duct at 1 kHz is given by $(0.0858 - 0.045)/0.075 = 0.544$, where 0.0858 m is a quarter of the wavelength and 0.075 m is the radius of the duct. This value of end correction is close to a value 0.0525 which may be calculated using plane wave theory; the small discrepancy is caused by the fact that the anti-node position in Figure 7 is influenced by the evanescent modes rather than assuming purely plane wave propagation.

5 Conclusion

A hybrid finite element model is used here to compute the instantaneous and time independent complex intensity within an open ended duct with an infinite flange. Theoretical predictions are compared with a "p-u" Microflown [8] intensity probe and here good agreement between prediction and measurement is observed in the plane wave regime of the duct. Furthermore, it is shown that for the experimental measurements the method of Schiffrer and Stanzial [4] is the most useful when it comes to capturing the complex sound intensity field in the duct, whereas the method of Heyser [3] only delivers a rolling average of the sound intensity. Accordingly, it appears viable in the future to adopt the method of Schiffrer and Stanzial, and later articles [5, 6], to investigate the effect of the presence, say, of blockages or other area discontinuities such as ductwork systems on the complex intensity field in a duct

Acknowledgments

The authors would like to thank the UK Technology Strategy Board (TSB), through the Knowledge Transfer Programme (KTP), for their support of the work reported in this article.

References

[1] F. J. Fahy, Sound intensity, E & FN Spon, (1995).

[2] F. Jacobsen, "A note on instantaneous and time-averaged active and reactive sound intensity," J. Sound Vib. 147(3), 489-496 (1991).

[3] R. C. Heyser. Instantaneous intensity. 81st Convention. Los Angeles, California (1986).

[4] G. Schiffrer and D. Stanzial, "Energetic properties of acoustic fields," J. Acoust. Soc. Am. 96(6), 3645-3653 (1994).

[5] D. Stanzial, N. Prodi, and G. Schiffrer, "Reactive acoustic intensity for general fields and energy polarization," J. Acoust. Soc. Am. 99(4), 1868-1876 (1996).

[6] D. Stanzial and N. Prodi, "Measurements of newly defined intensimetric quantities and their physical interpretation," J. Acoust. Soc. Am. 102(4), 2033-2039 (1997)

[7] R. Kirby, "Modeling sound propagation in acoustic waveguides using a hybrid numerical method," J. Acoust. Soc. Am. 124(4), 1930-1940 (2008).

[8] www.microflown.com